Journal of Alloys and Compounds 900 (2022) 163559

Contents lists available at ScienceDirect

Journal of Alloys and Compounds

journal homepage: www.elsevier.com/locate/jalcom

Preparation of porous TiNi-Ti alloy by diffusion sintering method and study of its composition, structure and martensitic transformations

Sergey G. Anikeev[a,*], Nadezhda V. Artyukhova[a], Anastasiia V. Shabalina[a], Sergei A. Kulinich[b,c], Valentina N. Hodorenko[a], Maria I. Kaftaranova[a], Vladimir V. Promakhov[a], Victor E. Gunter[a]

[a] Tomsk State University, Lenin Ave. 36, Tomsk 634050, Russia
[b] Tokai University, Research Institute of Science and Technology, Hiratsuka, Kanagawa 250-1292, Japan
[c] Far Eastern Federal University, Vladivostok 690041, Russia

ARTICLE INFO

Article history:
Received 9 November 2021
Received in revised form 24 December 2021
Accepted 30 December 2021
Available online 31 December 2021

Keywords:
TiNi
Porous alloy
Ti additives
Powder metallurgy
Martensitic transformations
Materials for implants

ABSTRACT

The study demonstrates a method for controlling not only the phase composition but also the atomic composition of TiNi matrix in porous TiNi-Ti alloys developed for biomedical uses as implants. The alloys were obtained from TiNi powder which was sintered with Ti powder added at as much as 0–10 at%. The structure, phase and chemical composition of the produced TiNi-Ti alloys was investigated with respect to the amount of Ti added into the material. It is shown that in the sintered product containing 5 at% and more of Ti additive, the composition of its TiNi matrix becomes close to equiatomic (with Ti:Ni atomic ratio ~1), and the excessive Ti precipitates as secondary phases Ti_2Ni and Ti_3Ni_4. In parallel, with increase in Ti additive from 0–10 at%, the structure of the precipitating Ti_2Ni type phases changes its morphology from separate spherical or pyramidal precipitates to large dendritic formations. The direct martensitic transformation from austenite to martensite in all the samples was found to proceed in two stages and through the *R*-phase (*B2*→*R*→*B19′*). Thermoresistive analysis demonstrated that TiNi-Ti samples with 5 and more at% of Ti had their characteristic starting temperature of martensite transition stabilizing at ~57 °C (330 K). This implies that the sample with 5 at% of Ti additive exhibited desired martensite transition temperatures, while containing a minimum concentration of secondary-phase precipitates in its matrix which deteriorate its properties. Thus, for the first time, we show that a very simple preparation approach based on sintering powders of TiNi and Ti is capable of producing porous TiNi-Ti alloys with properties optimized for fabricating bone implants.

1. Introduction

Titanium nickelide (TiNi) alloys are well-known to have martensitic transformations (MTs) that underlie their shape-memory effect and super-elasticity [1]. Porous TiNi shape-memory alloys (SMAs) still exhibit the unique properties of their bulk counterparts [2]. That is why they are promising biomedical materials for orthopedics and bone implant surgery, since they allow for tissue ingrowth and bone fixation, also providing the possibility for body fluids to flow [3]. Several methods for preparation of such materials are described in the literature, all being based on conventional powder metallurgy fabrication routes [4], such as sintering [5], self-propagating high-temperature synthesis in its layer-by-layer synthesis mode [6,7] or as thermal explosion combustion [8] of Ti and Ni powders, thermohydration process [9], selective laser sintering [10], and hot isostatic pressing (HIP) [11]. In this work, we deal with porous TiNi alloys obtained via the diffusion sintering method from a pre-prepared TiNi powder obtained using calciothermic reduction method [12,13].

For the sake of compatibility and to make them more functional, there were even attempts to develop porous TiNi materials that mimic natural patterns/materials [14]. Yet, the main important requirement for such porous implants is their high porosity (30–90%) [15], while such factors as pore size, permeability, surface area, mechanical performance (shear stress) and functional characteristics (MT temperatures and mechanisms) are still important for implant applications and have to be optimized for newly developed materials [16–18].

The characteristic MT temperatures (M_s, M_f, A_s, and A_f) of TiNi alloys are determined by their ratio Ti:Ni, as well as by aging

* Corresponding author.
E-mail address: anikeev_sergey@mail.ru (S.G. Anikeev).

https://doi.org/10.1016/j.jallcom.2021.163559
0925-8388/

treatment, mechanical treatment (cold-working), thermomechanical treatments, addition of a third element, point defects, dislocations and degree of order/disorder, secondary-phase particles, and alloying [1,15,19,20]. Noteworthy, both the atomic composition of the TiNi matrix and the amount, composition and structural features of secondary-phase precipitates are important for functional properties of SMAs.

In turn, all the above properties are determined by the initial powder(s) from which the porous material is prepared, as well as by process conditions, both being key factors governing the structural and compositional features of obtained product. Preparation of bulk (also known as 'solid' or 'compact') TiNi SMAs *via* diffusion sintering methods using pre-prepared TiNi powders makes it possible to reduce the inhomogeneity of their phase-chemical composition [21,22]. However, when a porous TiNi SMA is prepared *via* sintering a one-component TiNi powder system, the Ti content in its TiNi matrix decreases during high-temperature treatment [23]. This happens due to segregation of Ti atoms along free surfaces [24], oxidation processes [24], and formation of Ti_2Ni and Ti_4Ni_2(O,N,C) secondary phases [25]. Thus, the Ti:Ni ratio in produced porous TiNi SMAs changes toward Ti depletion. As a result, the MT in such porous TiNi alloys is not complete up to temperatures as low as 123 K, which negatively affects their functional properties [26]. The above problem can be solved through the use of Ti additions to the basic TiNi powder [27].

In our previous study, for the first time, we introduced Ti additives to porous TiNi alloys during sintering [27]. Before, this type of additives was only applied to TiNi monoliths (see, for instance, work [28]). We mixed TiNi and Ti powders with the concentration of the latter powder being 5, 10, and 15 at% and studied characteristic structural features of porous materials obtained after sintering. We showed that this method of Ti introduction could correct the composition of TiNi matrix, while the increase of Ti additive was found to lead to larger amounts of Ti_2Ni and Ti_4Ni_2(O,N,C) secondary phases in the matrix. However, no systematic studies on the composition of prepared materials and relationship between the formed structure and its MTs were presented. Therefore, for the first time, the present work focused on optimising TiNi-Ti alloys obtained by sintering TiNi and Ti powders, aiming at producing porous alloys with properties appropriate for bone implants. Keeping this in mind, we obtained porous TiNi-Ti alloys with Ti additives of 2.5, 5, 7.5, and 10 at% and investigated their morphological composition, structure and MT features. In other words, the main motivation of this work was finding optimal conditions that permit to produce a porous TiNi-Ti alloy with an attractive combination of (i) porosity, (ii) Ti:Ni atomic ratio in its matrix close to equiatomic, and (iii) temperatures of martensitic transitions close to those in human body.

2. Materials and methods

Experimental TiNi samples with Ti additives were obtained by diffusion sintering from TiNi (PV-N55T45) and Ti (PTEM-1) powders. The concentration range of Ti additive studied was from 0 to 10 at%, with a step being of 2.5 at%. Hereafter, the fabricated samples are denoted as TiNi-nTi, where *n* is the percentage of Ti added. To prepare such TiNi-nTi samles, a TiNi powder with sizes within the range of 100–160 μm was used. The metallic Ti powder used had a dual-mode size distribution (with their ratio being 50/50), 160–200 μm and less than 100 μm, with particle sizes being determined through sieve analysis. The exact amount of each fraction used for each sample is presented in Table S1 (Supplementary Material).

The initial powder components were dried, mixed, and filled (with an initial porosity evaluated as 60–70%) into quartz capsules with an inner diameter of 13–14 mm and a length of 65–80 mm. Sintering of capsules was carried out in a horizontal position in an electric vacuum furnace SNVE-1.31/16-I4 for 15 min at the temperature of 1255 ± 5 °C.

X-ray diffraction study of the samples was carried out on an XRD 6000 (Shimadzu, Japan) and ARL X'TRA (Thermo Fisher Scientific, Switzerland) diffractometers with CuKα radiation within the range of 2θ = 20–100° and at a rate of 0.02°/s. The PDF-4 database and Powder Cell 2.5 software with pseudo-Voigt profile function were used for phase analysis. Elemental composition was studied by energy-dispersive X-ray spectroscopy (EDX) using an energy dispersive spectrometer EDAX ECON IV (Amitek Inc., USA).

Structural features of fabricated alloys were studied by scanning electron microscopy (SEM) in the mode of secondary (SE) and backscatter electrons (BSE) on a microscope Quanta 200 3D and by transmission electron microscopy (TEM) on a microscope Hitachi HT-7700 equipped with a scanning mode unit and a Bruker X-Flash 6 T/60 V energy-dispersive spectrometer. For TEM, cross-sectional samples were prepared from pore walls using a Hitachi FB-2100 focused ion beam (FIB) system.

The sequence and characteristic temperatures of MT were determined by studying temperature dependence of electrical resistance, ER, (SIES-30). The method of differential scanning calorimetry, DSC (Netzsch DSC 404 F3), was applied for thermal transitions studies. Experimental samples for ER and DSC studies with dimensions 45 × 5 × 1 mm^3 and 3 × 3 × 1 mm^3 were prepared using an electro-discharge machine (ARTA 153). In all the above measurements, temperature inaccuracy was within ± 2 K.

3. Results and discussion

3.1. Preparation of porous structure

In this work, the upper threshold of Ti additive was limited to 10 at%, since adding larger amounts of Ti powder into the TiNi-Ti system under the same preparation conditions was shown earlier to result in a monolithic rather than porous structure [27]. It was also shown that the selected temperature-time regime, which was employed in this study, permitted to obtain porous materials based on TiNi with an optimal degree of sintering [27].

According to the recent work of Peng and co-authors, a synergistic effect was observed between pores and interactions of TiNi matrix with its embedded Ti_2Ni particle-like structures [5]. The obtained material was reported to exhibit ultrahigh damping and superelasticity [5]. That is why porosity and its morphology are extremely important issues for every newly-prepared TiNi-Ti material developed for implants.

As described above, several different methods are used to obtain porous TiNi SMAs. For example, in work [4] porous material with pure austenite phase was fabricated using a conventional powder-metallurgy route. However, because of its low porosity (21–26%) and too small pores (4–65 μm), the material was not found suitable for bone replacement applications. TiNi SAM with Ti_2Ni secondary-phase particles in its structure and porosity of 37% was obtained by sintering of Ti and Ni powders in work [5]. The authors of work [9] reported on a thermohydration process to produce porous TiNi. The obtained material exhibited a homogenous structure, isotropic pore morphology, and Young's modulus close to that of natural cortical bone, while the porosity was somewhat low (on the order of 40%) [9]. Another group prepared TiNi from Ti and Ni powders *via* the thermal explosion combustion method, using a Ti powder of 40 μm in size and Ni powders with sizes of 90, 40, 10 and 1.2 μm [8]. The reactive sintering behavior of such Ti-Ni mixtures depending on the fraction of Ni powder and process conditions were studied [8]. As a result, this permitted to develop recipes for preparation of porous or dense TiNi, respectively, for biomedical or actuator applications [8].

In the present work, an additional goal was to obtain materials with a highest possible coefficient of porosity (under conditions

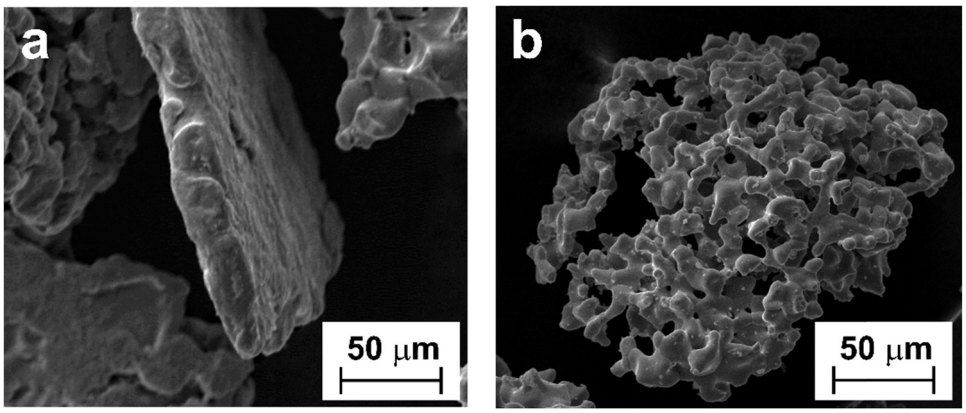

Fig. 1. SEM images of TiNi particles comprising the initial powder, with (a) compact (sizes 160–200 μm) and (b) spongy morphology (fractions 100–160 μm and < 100 μm).

used) that fully corresponds to the macrostructure of bone tissues in human body, which could not be achieved earlier. Our experiments demonstrated that when the initial TiNi powder with larger sizes (160–200 μm) was used, the initial porosity of material prior to thermal treatment was about 60%. Taking into account shrinkage after sintering, such a product could not provide a highly porous material (with porosity over 60%). Surprisingly, materials prepared from the two remaining size fractions (of 100–160 μm and < 100 μm) could be more porous, reaching porosity values as high as 70%.

The larger particles with sizes 160–200 μm were found to have mainly compact morphology (Fig. 1a) with traces of deformation along one direction. In contrast, because the smaller TiNi particles used had a spongy morphology (Fig. 1b), they gave rise to products with an initial porosity of about 70%. However, a decrease in particle size of the initial TiNi powder below 100 μm was found to lead to pores with smaller sizes. This resulted in a lower permeability of the porous material for cells. That is why, in this study, materials were sintered from a TiNi powder with sizes 100–160 μm as we aimed at obtaining TiNi-Ti alloys with high both porosity and permeability.

When testing different fractions of Ti powder, it was found that all the fractions (160–200, 100–160, or < 100 μm) led to product porosity of around 60–70%. Therefore, we decided to use two fractions of Ti powder as additives for sintering with TiNi. The largest fraction (of 160–200 μm) was expected to form a framework structure inside the TiNi-Ti mixture, while smaller Ti particles (fraction with sizes < 100 μm) were added for a more uniform distribution of Ti additives in the final porous product.

Thus, to obtain porous TiNi with Ti additive, in this work three powders were used: TiNi powder of the middle fraction (100–160 μm) and Ti powders of large (160–200 μm) and fine (< 100 μm) fractions. The two Ti powder fractions were mixed and added in a ratio of 1:1.

3.2. Phase composition

All the porous TiNi-Ti samples obtained by diffusion sintering were found to have a similar phase composition irrespective of the amount of Ti particles added during their preparation. The data of XRD microanalysis (Fig. 2) show that all the alloys contain the austenite phase of TiNi (*B2*), martensitic phase of TiNi (*B19'*), as well as secondary phases of Ti_2Ni, Ti_3Ni_4, and $TiNi_3$. It was impossible to determine the volume fraction for each detected phase as the produced TiNi-Ti alloys were quite inhomogeneous. However, for the consolidated content of Ti_2Ni and $Ti_4Ni_2(O,N,C)$ phases (hereafter denoted as Ti_2Ni type for simplicity) this can be done using the stereometric technique. The fraction of Ti-rich phases must be considered because of their significant effect on the properties of the resulting TiNi material. For example, Ti_2Ni cubic crystals present in

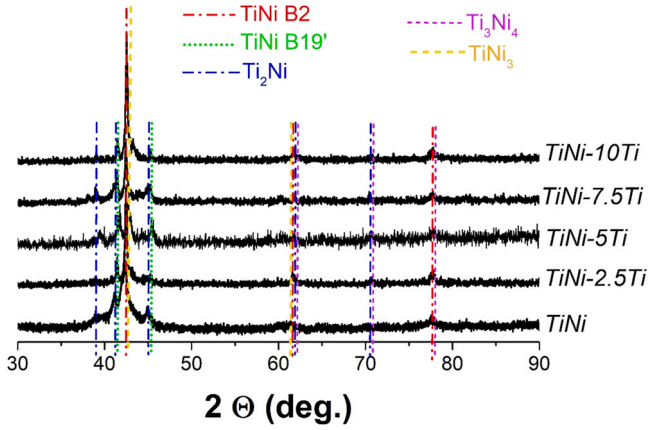

Fig. 2. XRD patterns obtained for porous TiNi-Ti alloys.

Ti-rich TiNi alloys were shown to affect both their shape memory and mechanical properties [29–31]. Lu et al. used heat treatment (*via* selective laser melting) to homogenize Ti_2Ni precipitates, thus optimizing mechanical properties of TiNi SMA (with 50.6 at% of Ti) [32].

The sintering temperatures used in this work were within the range of those favoring the formation of Ti_2Ni as a result of the liquid-phase interaction between the TiNi melt and Ti particles, in accordance with the equation: TiNi+Ti→Ti_2Ni. It is seen in Fig. 2 that with an increase in the amount of Ti additive, the content of the Ti_2Ni phase (together with that of $Ti_4Ni_2(O,N,C)$ phase) increased (Table 1). Its volume fraction was evaluated as 8.3%, 12.7%, 16.3%, and 25.3% for samples TiNi-2.5Ti, TiNi-5Ti, TiNi-7.5Ti, and TiNi-10Ti, respectively. It is seen that the amount of Ti additive used affected the Ti-rich phases content in the resulting material. Thus, when adding Ti to TiNi, one should optimize the composition of forming TiNi matrix and its Ti_2Ni content in order to avoid worsening the functional properties of the material.

Table 1
Chemical and phase composition of porous TiNi-Ti samples obtained from XRD and EDX.

Material	Ti additive (at%)	Ti_2Ni content (vol%)	Ti content in TiNi matrix (at%)
TiNi	0	6.0	46.5 ± 0.2
TiNi-2.5Ti	2.5	8.3	49.4 ± 0.2
TiNi-5Ti	5	12.7	49.7 ± 0.3
TiNi-7.5Ti	7.5	16.3	49.7 ± 0.3
TiNi-10Ti	10	25.3	49.8 ± 0.2

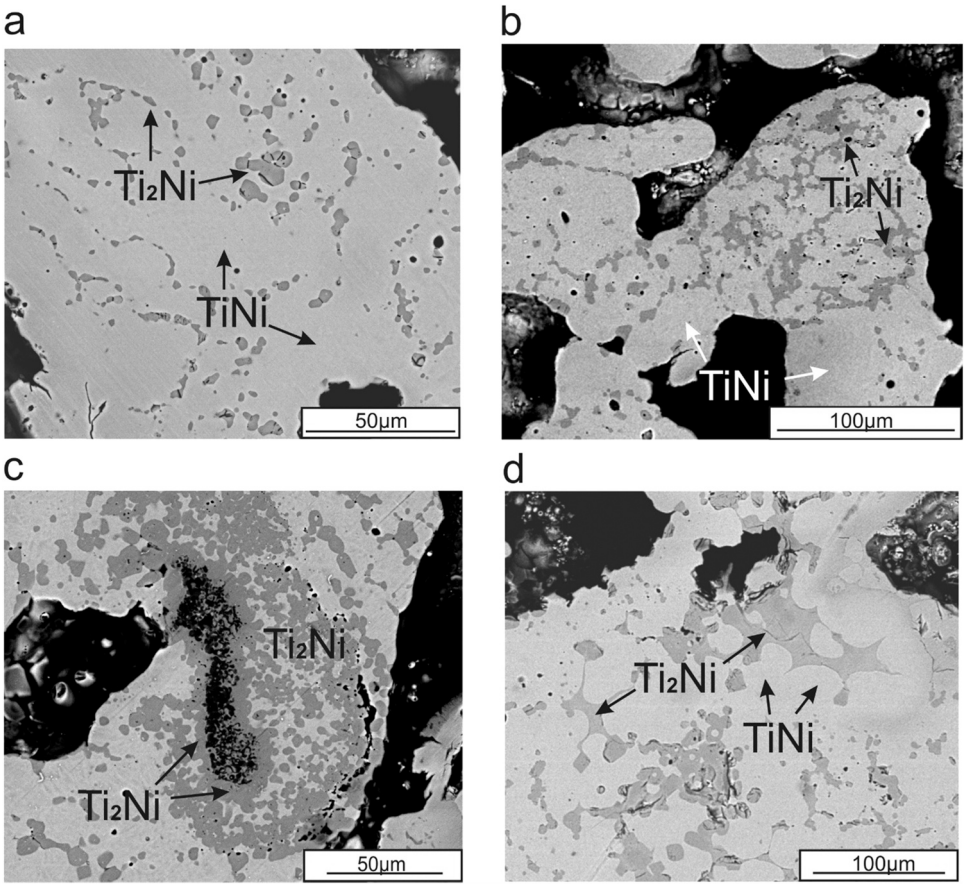

Fig. 3. Microstructure of porous TiNi alloy (a), and sintered TiNi-Ti alloys with Ti additive of 5 at% (b), 7.5 at% Ti (c), and 10 at% Ti (d). Thin section images of the alloys were taken in BSE mode.

3.3. SEM and EDX studies

SEM images obtained for thin sections of metallographic samples taken in the BSE mode are presented in Fig. 3, where the Ti_2Ni phase is seen as gray spots and regions. The collected images showed that as the atomic fraction of Ti additive increased from 0 to 10 at%, the phase of Ti_2Ni type was found to exhibit certain distinctive morphological features. In the alloy without Ti additive, the Ti_2Ni phase is seen in Fig. 3a to be presented in the form of separate round or pyramidal precipitates incorporated in the TiNi matrix and along grain boundaries.

In the structure of porous sample TiNi-5Ti, agglomerates of Ti_2Ni inclusions are mainly observed along grain boundaries as a result of coalescence of particles of the Ti_2Ni phase (Fig. 3b). With a further increase in the amount of Ti additive to 7.5 at%, the amount of Ti_2Ni melt is seen in Fig. 3c to increase during sintering. This melt involves individual large and small particles enriched in titanium, creating wide interlayers of the Ti_2Ni phase along pore boundaries and extensive accumulations of precipitates in the structure. Further increase in the amount of Ti additive is seen in Fig. 3d to lead to the formation of large dendritic structures of Ti_2Ni-TiNi consisting of TiNi grains and intergranular Ti_2Ni phase [33].

Based on EDX microanalysis, the composition of the TiNi matrix phase was established for all investigated materials, which was done based on the areas free from secondary-phase particles. For the alloy without Ti additives, its TiNi matrix had 46.5 ± 0.2 at% of Ti and 53.5 ± 0.2 at% of Ni (Table 1). The formation of Ti_2Ni particles [34], in combination with segregation of Ti on free surfaces [24] and formation of an amorphous TiO_2 layer (see Fig. 4b and its inset 6 below) leads to depletion in Ti of the TiNi compound and its enrichment in Ni. Introduction of a small amount of Ti additive (2.5 at%, sample TiNi-2.5Ti) is seen in Table 1 to shift the atomic content of Ti in TiNi to 49.4 at% (Table 1). Further addition of Ti powder into sintered mixture was found to increase the Ti content in the TiNi matrix of samples TiNi-5Ti and TiNi-7.5Ti to 49.7 ± 0.3 at%, which is close to equiatomic chemical composition. Interestingly, adding more Ti powder (10 at%, sample TiNi-10Ti) did not affect the composition of the TiNi matrix significantly as its Ti content was found to be 49.8 ± 0.2 at%. This observation is in agreement with our previous work, where further increase in the amount of Ti additive (over 10 at %) did not lead to changes in the ratio of components in the TiNi phase [27].

Thus, adding more than 5 at% of Ti additive into sintering mixture of TiNi-Ti does not affect the composition of TiNi matrix. This can be explained by the fact that, according to the state diagram of the Ti–Ni system, the solubility of Ti in TiNi is limited [26], and thus the excess of Ti atoms is used to form interlayers and particles based on Ti_2Ni and Ti_4Ni_2 (O,N,C) phases, as such phases have minimum formation enthalpy in the Ti–Ni system [35,36].

So, using different amounts of Ti additive permits to correct not only the phase composition of the porous alloy product but also the chemical composition of its TiNi matrix. The latter matrix is known to be responsible for the implementation of the martensitic transformation in the produced material and, accordingly, for its functional properties. And at this point, we assume that adding 5 at% of Ti leads to a nearly equiatomic TiNi matrix composition, while the alloy still has the smallest amount of Ti_2Ni phase in its TiNi matrix in comparison with samples TiNi-7.5Ti and TiNi-10Ti. However, this assumption still needs additional investigations of MTs in all the samples before sample TiNi-5Ti is proved to be the optimal one.

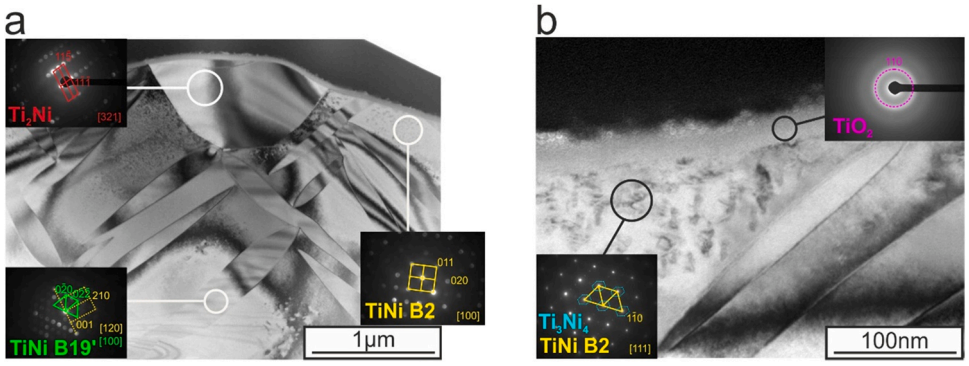

Fig. 4. Characteristic TEM images of sample TiNi-5Ti (a, b). Insets: SAED patterns of Ti_2Ni (red); TiNi *B19′* (green); TiNi B2 (yellow); Ti_3Ni_4 (blue); and TiO_2 (pink) (For interpretation of the references to colour in this figure legend, the reader is referred to the web version of this article).

Here, it is important to point at the structural and phase inhomogeneity observed in the prepared samples, and especially in those with higher amounts of Ti additive (see, for example, Fig. 3). Overall, the presence of quite large second-phase particles (mainly Ti_2Ni) incorporated all over the TiNi matrix points at its structural inhomogeneity. In principle, because of this, one can expect poorer mechanical properties of the material starting from some percentage of Ti additive. In this work, we observed significant inhomogeneity for samples with Ti addition of 7.5 and 10 at%. At the same time, addition of 5 at% of Ti and less was not found to result in the formation of a tangible amount of inhomogeneous areas. Such inhomogeneous areas presented in sample TiNi-7.5Ti are shown in greater detail in Fig. S1 (Supplementary Material). Preliminary results of mechanical tests indeed confirmed poorer properties of samples with Ti addition of 7.5 at% and more, while mechanical characteristics of the samples, as well as their optimization and detailed analysis, will be the subject of our next report as the corresponding research is now underway.

3.4. TEM studies

The finest microstructure of the prepared porous TiNi-Ti alloys was studied using TEM with SAED. All the samples were found to have a similar phase micro-composition. Combination of TEM images and their corresponding electron diffraction patterns permitted to detect and identify the following phases: TiNi (*B2*), TiNi (*B19′*), Ti_2Ni, Ti_3Ni_4 and a surface amorphous layer of TiO_2 (Fig. 4). For convenience, Fig. S2 (Supplementary Material) exhibits panel (a) from Fig. 4 where all these phases schematically marked with colors as they were found in sample TiNi-5Ti.

Surface modification of TiNi SMAs is quite often used to obtain thin layers of titanium oxide or/and nitride. Such layers protect the environment (body fluids, tissues, etc.) from Ni ion release which is quite undesired for implants based on TiNi [37,38]. Chu et al. showed that electro- and chemical polishing of commercially available TiNi SMA with 50.8 at% of Ni resulted in a thin surface layer (~10 nm) depleted of Ni and consisting of titanium oxide and suboxides (TiO, Ti_2O_3) [38]. Lelatko and co-authors prepared TiO_2/TiN layers on a commercial TiNi SMA with 50.6 at% of Ni using a glow discharge technique [37]. Hence, the presence of a thin TiO_x layer on the pore surface of the TiNi-Ti alloys obtained in this study may play a protective role when they are applied as implants.

Fig. 4 shows bright-field images with corresponding SAED patterns from secondary-phase particles. Characteristic diffraction contrast caused by the internal stress from the presence of fine Ti_3Ni_4 particles in the *B2* matrix is well seen around such particles (see inset 5 in Fig. 4b). The precipitates of coherent Ti_3Ni_4 particles are seen to be distributed both in the grain body and along grain boundaries, while the stress induced by their presence led to the formation of *B19′* martensite crystals, according to the Clapeyron-Clausius equation [26]. Thus, formation of martensite is seen to occur at locations of high internal stress due to precipitation of coherent phases enriched in nickel.

It is seen in Fig. 4a (inset 2) that lamellar monoclinic *B19′* martensite is available in sample TiNi-5Ti in various forms, both as separate lenticular and lamellar crystals. Martensite phases formed under deformation are known to differ from those formed under cooling by a more developed dislocation structure and smaller crystal sizes [39]. The size of *B19′* martensite crystals is seen in Fig. 4 to vary from 2 to several microns. Also, it can be noticed that the presence of twinned thin TiNi (*B19′*) crystals is a characteristic feature of alloys with titanium additives exceeding 2.5 at% of Ti (Fig. 5).

The discovered twinned structure of the B19′ martensitic phase corresponds to uniform shear with an invariant lattice [110] [15,40]. This micro-twinning is possible for all crystallographic systems of longitudinal and shear deformations. Perhaps it should be considered as a necessary mechanical micro-twinning which ensures compatibility of martensitic rearrangement in the structure of a *B2* austenite matrix. In accordance with EDX studies, with an increase in Ti addition to the TiNi-Ti mixture, the composition of TiNi matrix approaches its equiatomic ratio and the concentration of finely dispersed Ti_3Ni_4 phases decreases. This leads to a decrease in the elastic modulus of material. The MTs of the prepared materials are described in the next section.

Thus, two TiNi structures (*B2* and *B19′*) were found in the TiNi matrix of prepared porous TiNi-Ti alloys. Also, along with quite large particles of the Ti_2Ni type phase (according to SEM and EDX), the obtained TiNi-Ti materials contain fine Ti_3Ni_4 precipitates in their micro-structure and a very thin protective layer of amorphous TiO_2 on the surface.

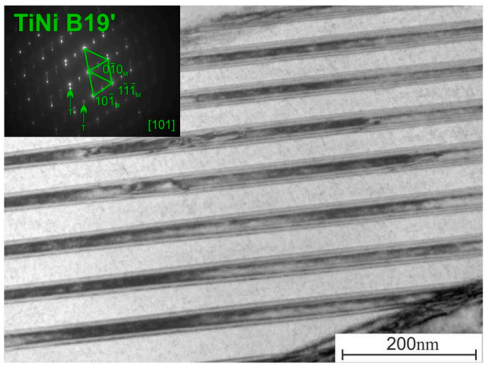

Fig. 5. TEM image of sample TiNi-10Ti, with a SAED pattern given as inset.

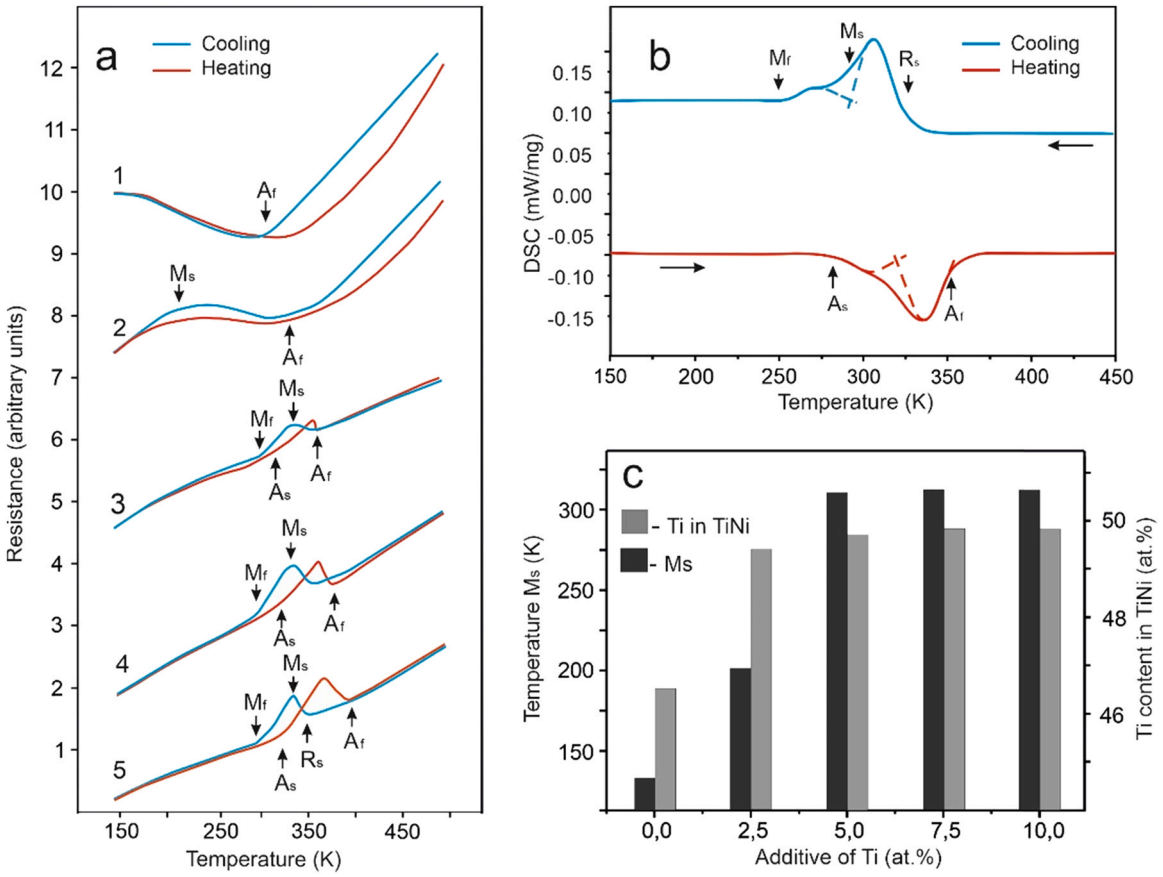

Fig. 6. (a) Temperature dependence of ER observed for porous TiNi-nTi samples with amount of Ti additive of 0 at% (1); 2.5 at% (2); 5 at% (3); 7.5 at% (4); and 10 at% (5). (b) Characteristic DSC curves for sample TiNi-5Ti. (c) Changes in M_s temperature as a function of the amount of Ti additive into sintered TiNi-Ti mixtures.

3.5. Martensitic transformations in prepared materials

In the present work, through the temperature dependence of electrical resistivity we found that the porous TiNi alloy without Ti additives demonstrated a wide temperature range of its direct MT. Compared with findings for its TiNi-Ti counterparts, the latter MT range was shifted to lower temperatures, not ending below 123 K (Fig. 6a, curve 1). This shift is believed to be associated with the enrichment of the TiNi matrix in Ni, as mentioned above (Section 3.2.). An additional reason for the observed low temperature M_s could be hardening caused by finely dispersed Ti_3Ni_4 particles (see inset 5 in Fig. 4b). Exhibiting high density, such precipitates become a barrier for the MT front during its propagation [41]. According to the rise in the level of electrical resistance in the alloy free of Ti additive, the direct MT goes through the *R*-phase. Thus, the martensitic transformation in the initial alloy is realized according to the sequence *B2*→*R*→*B19'* and at R_s and M_s temperatures of 270 and 130 K, respectively [42].

The martensitic transformation in aged materials based on titanium nickelide is known normally to proceed in two stages [43–45]. Based on the results of our resistivity measurements (see Fig. 6a) the first peak corresponds to the *B2*→*R* phase transition which is then followed by a *R*→*B19'* transition taking place after 20 K. Unlike the latter one, the former transition requires a small deformation of crystal lattice [41]. The transformation temperature interval between the two transitions is larger for porous alloys reaching as high as 100 K, which is explained by their chemical inhomogeneity [46].

On the other hand, a two-stage transition is also known to be characteristic for materials with increased contents of Ti_3Ni_4 phase and with grain sizes of 10–20 µm. In such materials, the reverse transformation *B19'*→*R* is sometimes realized in two stages, proceeding inside grains and at their boundaries at different temperatures and after different periods of time [47]. So, the two-stage MTs can be caused by either aging (including during heat treatment) of TiNi alloy or by the presence of Ti_3Ni_4 particles. In our materials, both cases are possible.

Adding 2.5 at% of Ti is seen in Fig. 6a (curve 2) to lead to an increase in characteristic temperatures with respect to the initial TiNi alloy while maintaining a wide range of MTs flowing through the R phase. As more (5 at%) Ti powder was mixed with TiNi before sintering, a clear M_s peak appears in the ER-temperature dependence of sample TiNi-5Ti (Fig. 6a, curve 3). It is quite broad but well seen when temperature dependence of this sample is compared with curves 1 and 2 in Fig. 6a.

With a further increase in Ti addition to 7.5 and to 10 at% (Fig. 6a, curves 4 and 5), the characteristic temperatures of the forward and reverse MT are seen to stabilize. This is believed to happen due to the equalization of the chemical composition of the TiNi matrix phase (see Table 1) which is responsible for the implementation of martensitic transformations in the material. Based on the shape and ER rise observed in Fig. 6a, the direct martensitic transformation from austenite to martensite in the TiNi samples sintered with 5–10 at% of Ti additive still proceeds in two stages, through the *R* phase.

Fig. 6c presents changes in MT temperatures depending on the amount of Ti additive sintered with TiNi powder, where light-gray and dark-gray bars stand for the amount of Ti additive and values of M_s achieved by samples, respectively. It is clear that addition of 5 at% of Ti is sufficient to correct the atomic composition of the TiNi

matrix in the entire bulk of the prepared porous alloys, thus providing them with MTs with operating temperatures close to that of human body.

The MT sequence and its temperature characteristics for sample TiNi-5Ti were thoroughly investigated by means of the DSC, with results being exhibited in Fig. 6b. The results are consistent with the ER-temperature dependence revealed for this sample in Fig. 6a (curve 3). The peak broadening observed in the process of phase transformation is characteristic of porous materials based on TiNi during heat release and heat absorption [46]. A characteristic feature of this dependence is the asymmetric nature of such peaks and their spreading. Adding 5 at% of Ti is seen in Fig. 6b to lead to a shift in the M_s temperature toward the *R* transformation, which results in an overlap of the peaks responsible for the transformations *B2*→*R* and *R*→*B19′*. As a consequence, a single asymmetric exothermic peak in the DSC curve is seen in Fig. 6b.

It is seen in Fig. 6 that the values of characteristic temperatures (in particular, R_s and M_s) were found to differ depending on the method used, ER or DSC. More specifically, for sample TiNi-5Ti, the difference observed for R_s and M_s was 20 and 40 K, respectively. This is explained by the porous structure of the samples, inhomogeneity of their chemical and phase composition, as well as certain instrumental peculiarities of the methods used. Note that the temperatures of MTs obtained from ER measurements agree well with those previously reported by others [40].

Thus, in accordance with the existing concepts for similar materials based on TiNi [48] and in light of the results of ER and DSC analyses (obtained for sample TiNi-5Ti), the present study demonstrates that two-stage MTs are realized in porous alloys produced *via* sintering of TiNi-Ti powders. Such MTs are shown to flow through the *R*-phase (*B2*→*R*→*B19′*) in the temperature range 340–273 K, which is consistent with the known concepts of temperature-dependent MTs reported for TiNi-based materials [20]. The first peak observed in the DSC curve for its heat release part (Fig. 6b, blue curve, dashed line) corresponds to the *B2*→*R* phase transition, which is then followed by the *R*→*B19′* transition (Fig. 6b, blue curve, dashed line). Likewise, for the DSC heat absorption curve. Similar phenomena were observed during heating stage (see red curve in Fig. 6b).

Thus, the MT temperatures achieved in the present study for samples TiNi-Ti sintered with Ti additives on the order of 5–10 at% seem to be attractive for using such materials as implants in human body. After adding ≥ 5 at% of Ti to sintered TiNi-Ti material, the TiNi matrix of the latter material reaches equiatomic chemical composition, with secondary phase particles of Ti_3Ni_4 as precipitates, thus resulting in the MT temperatures observed.

4. Conclusion

In this work, porous TiNi alloys were obtained via sintering TiNi and Ti powders with the latter powder added at the amount of 0, 2.5, 5, 7.5, and 10 at%. As a result, the product TiNi-Ti alloys exhibited porosity of 50–70% and average pore sizes of 60–100 μm (with minimum and maximum of 5 and 450 μm, respectively), i.e., characteristics attractive for biomedical bone implants. To prepare these materials via diffusion sintering, three powders were used: a TiNi powder of mid-sized fraction (100–160 μm) and Ti powders of large (160–200 μm) and fine (< 100 μm) fractions.

All prepared porous alloys were shown to contain two TiNi structures (*B2* and *B19′*) in their TiNi matrix, secondary phases (Ti_2Ni, Ti_3Ni_4, and $TiNi_3$) as fine precipitates, and a very thin protective layer of amorphous TiO_2 on their surface.

Increase in the amount of Ti additive was found to affect not only Ti-rich phases that precipitate within the TiNi matrix (the content of Ti_2Ni type phases rises with more Ti added) but also the chemical composition of the matrix itself, leading to almost equiatomic TiNi composition when 5 at% (or more) of Ti is added. Beginning from this point, when 5 at% and more of Ti is added into TiNi for sintering, the product's TiNi matrix reaches saturation and demonstrates ~ 49.7 at % of Ti. The remaining excess Ti contributes to the formation of secondary phases that precipitate as Ti_2Ni and Ti_3Ni_4.

At the same time, as the atomic fraction of Ti additive increased from 0 at% to 10 at%, the precipitating phase of Ti_2Ni type changes its morphology from separate spherical or pyramidal precipitates incorporated in the TiNi matrix and along grain boundaries (for TiNi without Ti additive) to large dendritic structures of Ti_2Ni-TiNi consisting of TiNi grains and intergranular Ti_2Ni phase (for samples with heavier Ti loads).

The direct austenite-to-martensite transformation was found to proceed in two stages and through the *R*-phase (*B2*→*R*→*B19′*) in all the samples, which was observed through resistance-temperature dependencies and then confirmed with differential scanning calorimetry. The TiNi material free of Ti additive exhibited its martensitic transformation range shifted to lower temperatures, not ending even at as low as 123 K. Adding just 2.5 at% of Ti to the sample immediately led to an increase in characteristic temperatures, while samples with 5 and more at% of Ti demonstrated a clear peak responsible for the start of martensitic transformation which stabilized at ~57 °C (330 K).

The presence of Ti_2Ni precipitates in the TiNi matrix is demonstrated to increase when more Ti powder is sintered with TiN powder, whereas such Ti-rich precipitates are known to affect the functional properties of targeted material. We show that in the sample sintered with 5 at% of Ti additive, a nearly equiatomic ratio Ti:Ni is reached in the matrix, while its content of Ti_2Ni precipitates is at minimum. Therefore, the sample demonstrates desired martensitic transformation temperatures, which implies that the method used is capable of producing porous TiNi-Ti alloys with properties optimized for applications as implants.

CRediT authorship contribution statement

Sergey G. Anikeev: Conceptualization, Investigation, Methodology, Project administration, Writing – original draft, Writing – review & editing. **Nadezhda V. Artyukhova:** Investigation, Validation, Formal analysis, Writing – original draft. **Anastasiia V. Shabalina:** Writing – original draft; writing – review & editing. **Sergei A. Kulinich:** Formal analysis, Writing – original draft, Writing – review & editing. **Valentina N. Hodorenko:** Methodology, Data curation, Formal analysis, Investigation. **Maria I. Kaftaranova:** Formal analysis, Investigation, Validation, Methodology. **Vladimir V. Promakhov:** Investigation, Validation. **Victor E. Gunter:** Conceptualization, Methodology, project administration, Writing – review & editing.

Declaration of Competing Interest

The authors declare that they have no known competing financial interests or personal relationships that could have appeared to influence the work reported in this paper.

Acknowledgments

This work was supported by the Russian Science Foundation (grant No. 19-79-10045). The electron microscopy studies were carried out using facilities of the Krasnoyarsk Regional Center for Collective Use, SB RAS.

Appendix A. Supporting information

Supplementary data associated with this article can be found in the online version at doi:10.1016/j.jallcom.2021.163559.

References

[1] C. Cismasiu, Shape Memory Alloys, Sciyo, Rijeka, Croatia, 2010, https://doi.org/10.5772/280

[2] S.B. Kang, K.S. Yoon, J.S. Kim, T.H. Nam, V.E. Gjunter, In vivo result of porous TiNi shape memory alloy: Bone response and growth, Mater. Trans. 43 (2002) 1045–1048.

[3] K. Sauli, Biocompatibility and Biomechanical Aspects of Nitinol Shape Memory Metal Implants, Department of Surgery, Department of Anatomy and Cell Biology, University of Oulu Press, Finland, 2003.

[4] T. Aydogmus, A.S. Bor, Production and characterization of porous TiNi shape memory alloys, Turk. J. Eng. Env. Sci. 35 (2011) 69–82, https://doi.org/10.3906/muh-1007-127

[5] W. Peng, K. Liu, B. Ali Shah, B. Yuan, Y. Gao, M. Zhu, Enhanced internal friction and specific strength of porous TiNi shape memory alloy composite by the synergistic effect of pore and Ti_2Ni, J. Alloy. Compd. 816 (2020) 152578, https://doi.org/10.1016/j.jallcom.2019.152578

[6] N. Resnina, V. Rubanik, V. Rubanik, M. Kulak, S. Belyaev, P. Liulchak, V. Kalganov, Influence of the Ar pressure on the structure of the NiTi foams produced by self-propagating high-temperature synthesis, Mater. Lett. 299 (2021) 130047.

[7] N. Resnina, S. Belyaev, A. Voronkov, Functional properties of porous Ti-48.0 at% Ni shape memory alloy produced by self-propagating high-temperature synthesis, J. Mater. Eng. Perform. 27 (2018) 1257–1264.

[8] M. Whitney, S.F. Corbin, R.B. Gorbet, Investigation of the influence of Ni powder size on microstructural evolution and the thermal explosion combustion synthesis of NiTi, Intermetallics 17 (2009) 894–906, https://doi.org/10.1016/j.intermet.2009.03.018

[9] S.K. Sadrnezhaad, S.A. Hosseini, Fabrication of porous NiTi-shape memory alloy objects by partially hydride titanium powder for biomedical applications, Mater. Des. 30 (2009) 4483–4487, https://doi.org/10.1016/j.matdes.2009.05.034

[10] I.V. Shishkovsky, L.T. Volova, M.V. Kuznetsov, Y.G. Morozov, I.P. Parkin, Porous biocompatible implants and tissue scaffolds synthesized by selective laser sintering from Ti and NiTi, J. Mater. Chem. 18 (2008) 1309–1317.

[11] D.C. Lagoudas, E.L. Vandygriff, Processing and characterization of NiTi porous SMA by elevated pressure sintering, J. Intel. Mater. Syst. Struct. 13 (2002) 837–850.

[12] S. Anikeev, V. Hodorenko, T. Chekalkin, V. Gunther, J. Kang, J. Kim, Fabrication and study of double sintered TiNi-based porous alloys, Smart Mater. Struct. 26 (2017) 057001.

[13] A.V. Kasimtsev, G.V. Markova, A. Shuitcev, Yu.V. Levinskii, T. Sviridova, A. Alpatov, Change in structure during consolidation of calcium hydride powders of TiNi, intermetallic, Metallurgist 58 (2015) 1038–1045.

[14] N. Ikeo, T. Matsumi, T. Ishimoto, R. Ozasa, A. Matsugaki, T. Matsuzaka, O. Gokcekaya, Y. Takigawa, T. Nakano, Fabrication of Ti-alloy powder/solid composite with uniaxial anisotropy by introducing unidirectional honeycomb structure via electron beam powder bed fusion, Crystals 11 (2021) 1074, https://doi.org/10.3390/cryst11091074

[15] B. Yuan, M. Zhu, C.Y. Chung, Biomedical porous shape memory alloys for hard-tissue replacement materials, Materials 11 (2018) 1716, https://doi.org/10.3390/ma11091716

[16] J. Li, D. Chen, H. Luan, Y. Zhang, Y. Fan, Numerical evaluation and prediction of porous implant design and flow performance, BioMed. Res. Int. 2018 (2018) 1215021, https://doi.org/10.1155/2018/1215021

[17] L.M.R. de Vasconcellos, D.O. Leite, F.N. de Oliveira, Y.R. Carvalho, C.A.A. Cairo, Evaluation of bone ingrowth into porous titanium implant: histomorphometric analysis in rabbits, Braz. Oral. Res. 24/4 (2010) 399–405.

[18] Y. Yao, Y. Yang, Q. Ye, S. Cao, X. Zhang, K. Zhao, Y. Jian, Effects of pore size and porosity on cytocompatibility and osteogenic differentiation of porous titanium, J. Mater. Sci.: Mater. Med. 32 (2021) 72, https://doi.org/10.1007/s10856-021-06548-0

[19] A. Bansiddhi, T.D. Sargeant, S.I. Stupp, D.C. Dunand, Porous NiTi for bone implants: a review, Acta Biomater. 4 (2008) 773–782, https://doi.org/10.1016/j.actbio.2008.02.009

[20] K. Otsuka, X.B. Ren, Recent developments in the research of shape memory alloys, Intermetallics 7 (1999) 511–528.

[21] G. Ryan, A. Pandit, D.P. Apatsidis, Fabrication methods of porous metals for use in orthopaedic applications, Biomaterials 27 (2006) 2651–2670, https://doi.org/10.1016/j.biomaterials.2005.12.002

[22] X. Liu, S. Wu, K.W. Yeung, Y.L. Chan, T. Hu, Z. Xu, X. Liu, J.C. Chung, K.M. Cheung, P.K. Chu, Relationship between osseointegration and superelastic biomechanics in porous NiTi scaffolds, Biomaterials 32 (2011) 330–338.

[23] G. Tosun, L. Ozler, M. Kaya, N.J. Orhan, A study on microstructure and porosity of NiTi alloy implants produced by SHS, J. Alloy. Compd. 478 (2009) 605–611, https://doi.org/10.1016/j.jallcom.2009.08.023

[24] S.L. Zhu, X.J. Yang, D.Z. Cui, Stress–strain behavior of porous NiTi alloys prepared by powders sintering, Mater. Sci. Eng. A 408 (2005) 264–268, https://doi.org/10.1016/j.msea.2005.08.012

[25] B. Yuan, C.Y. Chung, Y. Zhu, Microstructure and martensitic transformation behavior of porous NiTi shape memory alloy prepared by hot isostatic pressing processing, Mater. Sci. Eng. A. 382 (2004) 181–187, https://doi.org/10.1016/j.msea.2004.04.068

[26] Y. Zhao, M. Taya, Y. Kang, Compression behavior of porous NiTi shape memory alloy, Acta Mater. 53 (2005) 337–343, https://doi.org/10.1016/j.actamat.2004.09.029

[27] S.G. Anikeev, M.I. Kaftaranova, V.N. Khodorenko, N.V. Artyukhova, A.S. Garin, V.E. Gyunter, Effect of titanium additions on structural aspects of porous TiNi-based materials prepared by diffusion sintering, Inorg. Mater. 56 (9) (2020) 918–923.

[28] S. Shiva, I.A. Palani, S.K. Mishra, C.P. Paul, L.M. Kukreja, Investigations on the influence of composition in the development of Ni–Ti shape memory alloy using laser based additive manufacturing, Opt. Laser Technol. 69 (2015) 44–51, https://doi.org/10.1016/j.optlastec.2014.12.014

[29] M.H. Elahinia, M. Hashemi, M. Tabesh, S.B. Bhaduri, Manufacturing and processing of NiTi implants: A review, Prog. Mater. Sci. 57 (5) (2012) 911–946, https://doi.org/10.1016/j.pmatsci.2011.11.001

[30] J. Ma, I. Karaman, R.D. Noebe, High temperature shape memory alloys, Int. Mater. Rev. 55/5 (2010) 257–315, https://doi.org/10.1179/095066010×12646898728363

[31] H.Z. Lu, C. Yang, X. Luo, H.W. Ma, B. Song, Y.Y. Li, L.C. Zhang, Achieving ultrahigh-strength in beta-type titanium alloy by controlling the melt pool mode in selective laser melting, Mater. Sci. Eng. A 763 (2019) 138166, https://doi.org/10.1016/j.msea.2021.141731

[32] H.Z. Lu, L.H. Liu, C. Yang, X. Luo, C.H. Song, Z. Wang, J. Wang, Y.D. Su, Y.F. Ding, L.C. Zhang, Y.Y. Lia, Simultaneous enhancement of mechanical and shape memory properties by heat-treatment homogenization of Ti_2Ni precipitates in TiNi shape memory alloy fabricated by selective laser melting, J. Mater. Sci. Technol. 101 (2022) 205–216, https://doi.org/10.1016/j.jmst.2021.06.019

[33] P. Bartolo, J.P. Kruth, J. Silva, G. Levy, A. Malshe, K. Rajurkar, M. Mitsuishi, J. Ciurana, M. Leu, Biomedical production of implants by additive electro-chemical and physical processes, CIRP J. Manuf. 61 (2012) 635–655, https://doi.org/10.1016/j.cirp.2012.05.005

[34] J.Y. Xiong, C.Y. Li, X.J. Wang, P.D. Hodgson, C.E. Wen, Titanium-nickel shape memory alloy foams for bone tissue engineering, J. Mech. Behav. Biomed. 1 (2008) 269–273.

[35] J. Zhang, G. Fan, Y. Zhou, X. Ding, K. Otsuka, K. Nakamura, J. Sun, X. Ren, Does order–disorder transition exist in near-stoichiometric Ti–Ni shape memory alloys? Acta Mater. 55 (2007) 2897–2905.

[36] I. Saldan, J. Frenzel, O. Shekhah, R. Chelmowski, A. Birkner, Ch.Wolla, Surface of Ti–Ni alloys after their preparation, J. Alloy. Compd. 330- 332 (2009) 568–573.

[37] J. Lelatko, M. Freitag, J. Rak, T. Wierzchon, T. Goryczka, Structure of nitride and nitride/oxide layers formed on NiTi alloy, Solid State Phenom. 186 (2012) 259–262, https://doi.org/10.4028/www.scientific.net/SSP.186.259

[38] C.L. Chu, R.M. Wang, T. Hua, L.H. Yin, Y.P. Pu, P.H. Lin, S.L. Wu, C.Y. Chung, K.W.K. Yeung, P.K. Chu, Surface structure and biomedical properties of chemically polished and electropolished NiTi shape memory alloys, Mater. Sci. Eng. C. 28 (2008) 1430–1434, https://doi.org/10.1016/j.msec.2008.03.009

[39] E.Yu Panchenko, Yu.I. Chumlyakov, I.V. Kireeva, A.V. Ovsyannikov, H. Sehitoglu, I. Karaman, Y.H.J. Maier, Effect of disperse Ti3N4 particles on the martensitic transformations in titanium nickelide single crystals, Phys. Met. Metallogr. 106 (6) (2008) 577–589.

[40] K. Otsuka, X. Ren, Physical metallurgy of Ti–Ni-based shape memory alloys, Prog. Mater. Sci. 50 (2005) 511–678, https://doi.org/10.1016/j.pmatsci.2004.10.001

[41] M. Oghbaei, O.J. Mirzaee, Microwave versus conventional sintering: a review of fundamentals, advantages and applications, J. Alloy. Compd. 494 (2010) 175–189, https://doi.org/10.1016/j.jallcom.2010.01.068

[42] R. Roy, D. Agrawal, J. Cheng, S. Gedevanishvili, Full Sintering of powdered-metal bodies in a microwave field, Nature 399 (1999) 668–670.

[43] C.Y. Tang, L.N. Zhang, C.T. Wong, K.C. Chan, T.M. Yue, Fabrication and characteristics of porous NiTi shape memory alloy synthesized by microwave sintering, Mater. Sci. Eng. A 528 (2011) 6006–6011.

[44] T.W. Duerig, K. Bhattacharya, The influence of the R-phase on the superelastic behavior of NiTi, Shape Mem. Superelast. 1 (2015) 153–161, https://doi.org/10.1007/s40830-015-0013-4

[45] X.B. Wang, B. Verlinden, J. Van Humbeeck, R-phase transformation in NiTi alloys, Mater. Sci. Technol. 30 (2014) 1517–1529, https://doi.org/10.1179/1743284714y.0000000590

[46] V.E. Gunther, G.T. Dambaev, P.G. Sysolyatin , Delay law and new class of materials and implants in medicine, STT, Northampton, MA, 2000.

[47] C.Y. Tang, C.T. Wong, L.N. Zhang, M.T. Choy, T.W. Chow, K.C. Chan, T.M. Yue, Q. Chen, In situ formation of Ti alloy/TiC porous composites by rapid microwave sintering of Ti6Al4V/MWCNTs powder, J. Alloy. Compd. 557 (2013) 67–72, https://doi.org/10.1016/j.jallcom.2012.12.147

[48] J. Cheng, D. Agrawal, Y. Zhang, R. Roy, Microwave sintering of transparent alumina, Mater. Lett. 56 (2002) 587–592.